Search for the decay modes D-0 -> e(+) e(-), D-0 -> mu(+) mu(-), and D-0 -> e(+/-) mu -/+

Lees, J.P.; Raven, H.G.; BARBAR, Collaboration

published in
Physical Review D
2012

DOI (link to publisher)
10.1103/PhysRevD.86.032001

document version
Publisher's PDF, also known as Version of record

Search for the decay modes $D^0 \to e^+e^-$, $D^0 \to \mu^+\mu^-$, and $D^0 \to e^\pm\mu^\mp$

J. P. Lees,[1] V. Poireau,[1] V. Tisserand,[1] J. Garra Tico,[2] E. Grauges,[2] A. Palano,[3a,3b] G. Eigen,[4] B. Stugu,[4] D. N. Brown,[5] L. T. Kerth,[5] Yu. G. Kolomensky,[5] G. Lynch,[5] H. Koch,[6] T. Schroeder,[6] D. J. Asgeirsson,[7] C. Hearty,[7] T. S. Mattison,[7] J. A. McKenna,[7] R. Y. So,[7] A. Khan,[8] V. E. Blinov,[9] A. R. Buzykaev,[9] V. P. Druzhinin,[9] V. B. Golubev,[9] E. A. Kravchenko,[9] A. P. Onuchin,[9] S. I. Serednyakov,[9] Yu. I. Skovpen,[9] E. P. Solodov,[9] K. Yu. Todyshev,[9] A. N. Yushkov,[9] M. Bondioli,[10] D. Kirkby,[10] A. J. Lankford,[10] M. Mandelkern,[10] H. Atmacan,[11] J. W. Gary,[11] F. Liu,[11] O. Long,[11] E. Mullin,[11] G. M. Vitug,[11] C. Campagnari,[12] T. M. Hong,[12] D. Kovalskyi,[12] J. D. Richman,[12] C. A. West,[12] A. M. Eisner,[13] J. Kroseberg,[13] W. S. Lockman,[13] A. J. Martinez,[13] B. A. Schumm,[13] A. Seiden,[13] D. S. Chao,[14] C. H. Cheng,[14] B. Echenard,[14] K. T. Flood,[14] D. G. Hitlin,[14] P. Ongmongkolkul,[14] F. C. Porter,[14] A. Y. Rakitin,[14] R. Andreassen,[15] Z. Huard,[15] B. T. Meadows,[15] M. D. Sokoloff,[15] L. Sun,[15] P. C. Bloom,[16] W. T. Ford,[16] A. Gaz,[16] U. Nauenberg,[16] J. G. Smith,[16] S. R. Wagner,[16] R. Ayad,[17,*] W. H. Toki,[17] B. Spaan,[18] K. R. Schubert,[19] R. Schwierz,[19] D. Bernard,[20] M. Verderi,[20] P. J. Clark,[21] S. Playfer,[21] D. Bettoni,[22a] C. Bozzi,[22a] R. Calabrese,[22a,22b] G. Cibinetto,[22a,22b] E. Fioravanti,[22a,22b] I. Garzia,[22a] E. Luppi,[22a,22b] M. Munerato,[22a,22b] L. Piemontese,[22a] V. Santoro,[22a] R. Baldini-Ferroli,[23] A. Calcaterra,[23] R. de Sangro,[23] G. Finocchiaro,[23] P. Patteri,[23] I. M. Peruzzi,[23,†] M. Piccolo,[23] M. Rama,[23] A. Zallo,[23] R. Contri,[24a,24b] E. Guido,[24a,24b] M. Lo Vetere,[24a,24b] M. R. Monge,[24a,24b] S. Passaggio,[24a] C. Patrignani,[24a,24b] E. Robutti,[24a] B. Bhuyan,[25] V. Prasad,[25] C. L. Lee,[26] M. Morii,[26] A. J. Edwards,[27] A. Adametz,[28] U. Uwer,[28] H. M. Lacker,[29] T. Lueck,[29] P. D. Dauncey,[30] U. Mallik,[31] C. Chen,[32] J. Cochran,[32] W. T. Meyer,[32] S. Prell,[32] A. E. Rubin,[32] A. V. Gritsan,[33] Z. J. Guo,[33] N. Arnaud,[34] M. Davier,[34] D. Derkach,[34] G. Grosdidier,[34] F. Le Diberder,[34] A. M. Lutz,[34] B. Malaescu,[34] P. Roudeau,[34] M. H. Schune,[34] A. Stocchi,[34] G. Wormser,[34] D. J. Lange,[35] D. M. Wright,[35] C. A. Chavez,[36] J. P. Coleman,[36] J. R. Fry,[36] E. Gabathuler,[36] D. E. Hutchcroft,[36] D. J. Payne,[36] C. Touramanis,[36] A. J. Bevan,[37] F. Di Lodovico,[37] R. Sacco,[37] M. Sigamani,[37] G. Cowan,[38] D. N. Brown,[39] C. L. Davis,[39] A. G. Denig,[40] M. Fritsch,[40] W. Gradl,[40] K. Griessinger,[40] A. Hafner,[40] E. Prencipe,[40] R. J. Barlow,[41,‡] G. Jackson,[41] G. D. Lafferty,[41] E. Behn,[42] R. Cenci,[42] B. Hamilton,[42] A. Jawahery,[42] D. A. Roberts,[42] C. Dallapiccola,[43] R. Cowan,[44] D. Dujmic,[44] G. Sciolla,[44] R. Cheaib,[45] D. Lindemann,[45] P. M. Patel,[45,§] S. H. Robertson,[45] P. Biassoni,[46a,46b] N. Neri,[46a] F. Palombo,[46a,46b] S. Stracka,[46a,46b] L. Cremaldi,[47] R. Godang,[47,‖] R. Kroeger,[47] P. Sonnek,[47] D. J. Summers,[47] X. Nguyen,[48] M. Simard,[48] P. Taras,[48] G. De Nardo,[49a,49b] D. Monorchio,[49a,49b] G. Onorato,[49a,49b] C. Sciacca,[49a,49b] M. Martinelli,[50] G. Raven,[50] C. P. Jessop,[51] J. M. LoSecco,[51] W. F. Wang,[51] K. Honscheid,[52] R. Kass,[52] J. Brau,[53] R. Frey,[53] N. B. Sinev,[53] D. Strom,[53] E. Torrence,[53] E. Feltresi,[54a,54b] N. Gagliardi,[54a,54b] M. Margoni,[54a,54b] M. Morandin,[54a] M. Posocco,[54a] M. Rotondo,[54a] G. Simi,[54a] F. Simonetto,[54a,54b] R. Stroili,[54a,54b] S. Akar,[55] E. Ben-Haim,[55] M. Bomben,[55] G. R. Bonneaud,[55] H. Briand,[55] G. Calderini,[55] J. Chauveau,[55] O. Hamon,[55] Ph. Leruste,[55] G. Marchiori,[55] J. Ocariz,[55] S. Sitt,[55] M. Biasini,[56a,56b] E. Manoni,[56a,56b] S. Pacetti,[56a,56b] A. Rossi,[56a,56b] C. Angelini,[57a,57b] G. Batignani,[57a,57b] S. Bettarini,[57a,57b] M. Carpinelli,[57a,57b,¶] G. Casarosa,[57a,57b] A. Cervelli,[57a,57b] F. Forti,[57a,57b] M. A. Giorgi,[57a,57b] A. Lusiani,[57a,57c] B. Oberhof,[57a,57b] E. Paoloni,[57a,57b] A. Perez,[57a] G. Rizzo,[57a,57b] J. J. Walsh,[57a] D. Lopes Pegna,[58] J. Olsen,[58] A. J. S. Smith,[58] A. V. Telnov,[58] F. Anulli,[59a] R. Faccini,[59a,59b] F. Ferrarotto,[59a] F. Ferroni,[59a,59b] M. Gaspero,[59a,59b] L. Li Gioi,[59a] M. A. Mazzoni,[59a] G. Piredda,[59a] C. Bünger,[60] O. Grünberg,[60] T. Hartmann,[60] T. Leddig,[60] H. Schröder,[60,§] C. Voss,[60] R. Waldi,[60] T. Adye,[61] E. O. Olaiya,[61] F. F. Wilson,[61] S. Emery,[62] G. Hamel de Monchenault,[62] G. Vasseur,[62] Ch. Yèche,[62] D. Aston,[63] D. J. Bard,[63] R. Bartoldus,[63] J. F. Benitez,[63] C. Cartaro,[63] M. R. Convery,[63] J. Dorfan,[63] G. P. Dubois-Felsmann,[63] W. Dunwoodie,[63] M. Ebert,[63] R. C. Field,[63] M. Franco Sevilla,[63] B. G. Fulsom,[63] A. M. Gabareen,[63] M. T. Graham,[63] P. Grenier,[63] C. Hast,[63] W. R. Innes,[63] M. H. Kelsey,[63] P. Kim,[63] M. L. Kocian,[63] D. W. G. S. Leith,[63] P. Lewis,[63] B. Lindquist,[63] S. Luitz,[63] V. Luth,[63] H. L. Lynch,[63] D. B. MacFarlane,[63] D. R. Muller,[63] H. Neal,[63] S. Nelson,[63] M. Perl,[63] T. Pulliam,[63] B. N. Ratcliff,[63] A. Roodman,[63] A. A. Salnikov,[63] R. H. Schindler,[63] A. Snyder,[63] D. Su,[63] M. K. Sullivan,[63] J. Va'vra,[63] A. P. Wagner,[63] W. J. Wisniewski,[63] M. Wittgen,[63] D. H. Wright,[63] H. W. Wulsin,[63] C. C. Young,[63] V. Ziegler,[63] W. Park,[64] M. V. Purohit,[64] R. M. White,[64] J. R. Wilson,[64] A. Randle-Conde,[65] S. J. Sekula,[65] M. Bellis,[66] P. R. Burchat,[66] T. S. Miyashita,[66] E. M. T. Puccio,[66] M. S. Alam,[67] J. A. Ernst,[67] R. Gorodeisky,[68] N. Guttman,[68] D. R. Peimer,[68] A. Soffer,[68] P. Lund,[69] S. M. Spanier,[69] J. L. Ritchie,[70] A. M. Ruland,[70] R. F. Schwitters,[70] B. C. Wray,[70] J. M. Izen,[71] X. C. Lou,[71] F. Bianchi,[72a,72b] D. Gamba,[72a,72b] S. Zambito,[72a,72b] L. Lanceri,[73a,73b] L. Vitale,[73a,73b] F. Martinez-Vidal,[74] A. Oyanguren,[74] H. Ahmed,[75] J. Albert,[75] Sw. Banerjee,[75] F. U. Bernlochner,[75] H. H. F. Choi,[75] G. J. King,[75] R. Kowalewski,[75] M. J. Lewczuk,[75] I. M. Nugent,[75] J. M. Roney,[75] R. J. Sobie,[75] N. Tasneem,[75] T. J. Gershon,[76] P. F. Harrison,[76] T. E. Latham,[76] H. R. Band,[77] S. Dasu,[77] Y. Pan,[77] R. Prepost,[77] and S. L. Wu[77]

(*BABAR* Collaboration)

[1]*Laboratoire d'Annecy-le-Vieux de Physique des Particules (LAPP), Université de Savoie, CNRS/IN2P3, F-74941 Annecy-Le-Vieux, France*
[2]*Universitat de Barcelona, Facultat de Fisica, Departament ECM, E-08028 Barcelona, Spain*
[3a]*INFN Sezione di Bari, I-70126 Bari, Italy*
[3b]*Dipartimento di Fisica, Università di Bari, I-70126 Bari, Italy*
[4]*University of Bergen, Institute of Physics, N-5007 Bergen, Norway*
[5]*Lawrence Berkeley National Laboratory and University of California, Berkeley, California 94720, USA*
[6]*Ruhr Universität Bochum, Institut für Experimentalphysik 1, D-44780 Bochum, Germany*
[7]*University of British Columbia, Vancouver, British Columbia, Canada V6T 1Z1*
[8]*Brunel University, Uxbridge, Middlesex UB8 3PH, United Kingdom*
[9]*Budker Institute of Nuclear Physics, Novosibirsk 630090, Russia*
[10]*University of California at Irvine, Irvine, California 92697, USA*
[11]*University of California at Riverside, Riverside, California 92521, USA*
[12]*University of California at Santa Barbara, Santa Barbara, California 93106, USA*
[13]*University of California at Santa Cruz, Institute for Particle Physics, Santa Cruz, California 95064, USA*
[14]*California Institute of Technology, Pasadena, California 91125, USA*
[15]*University of Cincinnati, Cincinnati, Ohio 45221, USA*
[16]*University of Colorado, Boulder, Colorado 80309, USA*
[17]*Colorado State University, Fort Collins, Colorado 80523, USA*
[18]*Technische Universität Dortmund, Fakultät Physik, D-44221 Dortmund, Germany*
[19]*Technische Universität Dresden, Institut für Kern- und Teilchenphysik, D-01062 Dresden, Germany*
[20]*Laboratoire Leprince-Ringuet, Ecole Polytechnique, CNRS/IN2P3, F-91128 Palaiseau, France*
[21]*University of Edinburgh, Edinburgh EH9 3JZ, United Kingdom*
[22a]*INFN Sezione di Ferrara, I-44100 Ferrara, Italy*
[22b]*Dipartimento di Fisica, Università di Ferrara, I-44100 Ferrara, Italy*
[23]*INFN Laboratori Nazionali di Frascati, I-00044 Frascati, Italy*
[24a]*INFN Sezione di Genova, I-16146 Genova, Italy*
[24b]*Dipartimento di Fisica, Università di Genova, I-16146 Genova, Italy*
[25]*Indian Institute of Technology Guwahati, Guwahati, Assam, 781 039, India*
[26]*Harvard University, Cambridge, Massachusetts 02138, USA*
[27]*Harvey Mudd College, Claremont, California 91711, USA*
[28]*Universität Heidelberg, Physikalisches Institut, Philosophenweg 12, D-69120 Heidelberg, Germany*
[29]*Humboldt-Universität zu Berlin, Institut für Physik, Newtonstrasse 15, D-12489 Berlin, Germany*
[30]*Imperial College London, London, SW7 2AZ, United Kingdom*
[31]*University of Iowa, Iowa City, Iowa 52242, USA*
[32]*Iowa State University, Ames, Iowa 50011-3160, USA*
[33]*Johns Hopkins University, Baltimore, Maryland 21218, USA*
[34]*Laboratoire de l'Accélérateur Linéaire, IN2P3/CNRS et Université Paris-Sud 11, Centre Scientifique d'Orsay, B. P. 34, F-91898 Orsay Cedex, France*
[35]*Lawrence Livermore National Laboratory, Livermore, California 94550, USA*
[36]*University of Liverpool, Liverpool L69 7ZE, United Kingdom*
[37]*Queen Mary, University of London, London, E1 4NS, United Kingdom*
[38]*University of London, Royal Holloway and Bedford New College, Egham, Surrey TW20 0EX, United Kingdom*
[39]*University of Louisville, Louisville, Kentucky 40292, USA*
[40]*Johannes Gutenberg-Universität Mainz, Institut für Kernphysik, D-55099 Mainz, Germany*
[41]*University of Manchester, Manchester M13 9PL, United Kingdom*
[42]*University of Maryland, College Park, Maryland 20742, USA*
[43]*University of Massachusetts, Amherst, Massachusetts 01003, USA*
[44]*Massachusetts Institute of Technology, Laboratory for Nuclear Science, Cambridge, Massachusetts 02139, USA*
[45]*McGill University, Montréal, Québec, Canada H3A 2T8*
[46a]*INFN Sezione di Milano, I-20133 Milano, Italy*
[46b]*Dipartimento di Fisica, Università di Milano, I-20133 Milano, Italy*
[47]*University of Mississippi, University, Mississippi 38677, USA*
[48]*Université de Montréal, Physique des Particules, Montréal, Québec, Canada H3C 3J7*
[49a]*INFN Sezione di Napoli, I-80126 Napoli, Italy*
[49b]*Dipartimento di Scienze Fisiche, Università di Napoli Federico II, I-80126 Napoli, Italy*
[50]*NIKHEF, National Institute for Nuclear Physics and High Energy Physics, NL-1009 DB Amsterdam, The Netherlands*

[51]University of Notre Dame, Notre Dame, Indiana 46556, USA
[52]Ohio State University, Columbus, Ohio 43210, USA
[53]University of Oregon, Eugene, Oregon 97403, USA
[54a]INFN Sezione di Padova, I-35131 Padova, Italy
[54b]Dipartimento di Fisica, Università di Padova, I-35131 Padova, Italy
[55]Laboratoire de Physique Nucléaire et de Hautes Energies, IN2P3/CNRS, Université Pierre et Marie Curie-Paris6, Université Denis Diderot-Paris7, F-75252 Paris, France
[56a]INFN Sezione di Perugia, I-06100 Perugia, Italy
[56b]Dipartimento di Fisica, Università di Perugia, I-06100 Perugia, Italy
[57a]INFN Sezione di Pisa, I-56127 Pisa, Italy
[57b]Dipartimento di Fisica, Università di Pisa, I-56127 Pisa, Italy
[57c]Scuola Normale Superiore di Pisa, I-56127 Pisa, Italy
[58]Princeton University, Princeton, New Jersey 08544, USA
[59a]INFN Sezione di Roma, I-00185 Roma, Italy
[59b]Dipartimento di Fisica, Università di Roma La Sapienza, I-00185 Roma, Italy
[60]Universität Rostock, D-18051 Rostock, Germany
[61]Rutherford Appleton Laboratory, Chilton, Didcot, Oxon, OX11 0QX, United Kingdom
[62]CEA, Irfu, SPP, Centre de Saclay, F-91191 Gif-sur-Yvette, France
[63]SLAC National Accelerator Laboratory, Stanford, California 94309 USA
[64]University of South Carolina, Columbia, South Carolina 29208, USA
[65]Southern Methodist University, Dallas, Texas 75275, USA
[66]Stanford University, Stanford, California 94305-4060, USA
[67]State University of New York, Albany, New York 12222, USA
[68]Tel Aviv University, School of Physics and Astronomy, Tel Aviv, 69978, Israel
[69]University of Tennessee, Knoxville, Tennessee 37996, USA
[70]University of Texas at Austin, Austin, Texas 78712, USA
[71]University of Texas at Dallas, Richardson, Texas 75083, USA
[72a]INFN Sezione di Torino, I-10125 Torino, Italy
[72b]Dipartimento di Fisica Sperimentale, Università di Torino, I-10125 Torino, Italy
[73a]INFN Sezione di Trieste, I-34127 Trieste, Italy
[73b]Dipartimento di Fisica, Università di Trieste, I-34127 Trieste, Italy
[74]IFIC, Universitat de Valencia-CSIC, E-46071 Valencia, Spain
[75]University of Victoria, Victoria, British Columbia, Canada V8W 3P6
[76]Department of Physics, University of Warwick, Coventry CV4 7AL, United Kingdom
[77]University of Wisconsin, Madison, Wisconsin 53706, USA

(Received 26 June 2012; published 1 August 2012)

We present searches for the rare decay modes $D^0 \to e^+e^-$, $D^0 \to \mu^+\mu^-$, and $D^0 \to e^\pm\mu^\mp$ in continuum $e^+e^- \to c\bar{c}$ events recorded by the *BABAR* detector in a data sample that corresponds to an integrated luminosity of 468 fb^{-1}. These decays are highly Glashow–Iliopoulos–Maiani suppressed but may be enhanced in several extensions of the standard model. Our observed event yields are consistent with the expected backgrounds. An excess is seen in the $D^0 \to \mu^+\mu^-$ channel, although the observed yield is consistent with an upward background fluctuation at the 5% level. Using the Feldman–Cousins method, we set the following 90% confidence level intervals on the branching fractions: $\mathcal{B}(D^0 \to e^+e^-) < 1.7 \times 10^{-7}$, $\mathcal{B}(D^0 \to \mu^+\mu^-)$ within $[0.6, 8.1] \times 10^{-7}$, and $\mathcal{B}(D^0 \to e^\pm\mu^\mp) < 3.3 \times 10^{-7}$.

DOI: 10.1103/PhysRevD.86.032001 PACS numbers: 13.20.Fc, 11.30.Hv, 12.15.Mm, 12.60.−i

I. INTRODUCTION

In the standard model (SM), the flavor-changing neutral current decays $D^0 \to \ell^+\ell^-$ are strongly suppressed by the Glashow–Iliopoulos–Maiani mechanism. Long-distance processes bring the predicted branching fractions up to the order of 10^{-23} and 10^{-13} for $D^0 \to e^+e^-$ and $D^0 \to \mu^+\mu^-$ decays, respectively [1]. These predictions are well below current experimental sensitivities. The lepton-flavor violating decay $D^0 \to e^\pm\mu^\mp$ is forbidden in the SM. Several extensions of the SM predict $D^0 \to \ell^+\ell^-$ branching fractions that are enhanced by several orders of

*Now at the University of Tabuk, Tabuk 71491, Saudi Arabia.
†Also with Università di Perugia, Dipartimento di Fisica, Perugia, Italy.
‡Now at the University of Huddersfield, Huddersfield HD1 3DH, United Kingdom.
§Deceased.
‖Now at University of South Alabama, Mobile, AL 36688, USA.
¶Also with Università di Sassari, Sassari, Italy.

magnitude compared with the SM expectations [1]. The connection between $D^0 \to \ell^+\ell^-$ and D^0-$\bar{D}^0$ mixing in new physics models has also been emphasized [2].

We search for $D^0 \to \ell^+\ell^-$ decays using approximately 468 fb^{-1} of data produced by the PEP-II asymmetric-energy e^+e^- collider [3] and recorded by the *BABAR* detector. The center-of-mass energy of the machine was at, or 40 MeV below, the $\Upsilon(4S)$ resonance for this data set. The *BABAR* detector is described in detail elsewhere [4]. We give a brief summary of the main features below.

The trajectories and decay vertices of long-lived hadrons are reconstructed with a 5-layer, double-sided silicon strip detector (SVT) and a 40-layer drift chamber (DCH), which are inside a 1.5 T solenoidal magnetic field. Specific ionization (dE/dx) measurements are made by both the SVT and the DCH. The velocities of charged particles are inferred from the measured Cherenkov angle of radiation emitted within fused silica bars, located outside the tracking volume and detected by an array of phototubes. The dE/dx and Cherenkov angle measurements are used in particle identification. Photon and electron energy and photon position are measured by a CsI(Tl) crystal calorimeter (EMC). The steel of the flux return for the solenoidal magnet is instrumented with layers of either resistive plate chambers or limited streamer tubes [5], which are used to identify muons (IFR).

II. EVENT RECONSTRUCTION AND SELECTION

We form D^0 candidates by combining pairs of oppositely charged tracks and consider the following final states: e^+e^-, $\mu^+\mu^-$, $e^\pm\mu^\mp$, $\pi^+\pi^-$, and $K^-\pi^+$. We use the measured $D^0 \to \pi^+\pi^-$ yield and the known $D^0 \to \pi^+\pi^-$ branching fraction to normalize our $D^0 \to \ell^+\ell^-$ branching fractions. We also use the $D^0 \to \pi^+\pi^-$ candidates, as well as the $D^0 \to K^-\pi^+$ candidates, to measure the probability of misidentifying a π as either a μ or an e. Combinatorial background is reduced by requiring that the D^0 candidate originate from the decay $D^*(2010)^+ \to D^0\pi^+$ [6]. We select D^0 candidates produced in continuum $e^+e^- \to c\bar{c}$ events by requiring that the momentum of the D^0 candidate be above 2.4 GeV in the center-of-mass (CM) frame, which is close to the kinematic limit for $B \to D^*\pi$, $D^{*+} \to D^0\pi^+$. This reduces the combinatorial background from $e^+e^- \to B\bar{B}$ events.

Backgrounds are estimated directly from data control samples. Signal D^0 candidates with a reconstructed D^0 mass above 1.9 GeV consist of random combinations of tracks. We use a sideband region above the signal region in the D^0 mass ([1.90, 2.05] GeV) in a wide $\Delta m \equiv m(D^0\pi^+) - m(D^0)$ window ([0.141, 0.149] GeV) to estimate the amount of combinatorial background. The D^0 and Δm mass resolutions, measured in the $D^0 \to \pi^+\pi^-$ sample, are 8.1 MeV and 0.2 MeV, respectively. We estimate the number of $D^0 \to \pi^+\pi^-$ background events selected as $D^0 \to \ell^+\ell^-$ candidates by scaling the observed $D^0 \to \pi^+\pi^-$ yield, with no particle identification criteria applied, by the product of pion misidentification probabilities and a misidentification correlation factor G. The misidentification correlation factor G is estimated with the $D^0 \to K^-\pi^+$ data control sample.

The tracks for the D^0 candidates must have momenta greater than 0.1 GeV and have at least six hits in the SVT. The slow pion track from the $D^{*+} \to D^0\pi^+$ decay must have at least 12 position measurements in the DCH. A fit of the $D^{*+} \to D^0\pi^+$; $D^0 \to t^+t^-$ decay chain is performed where the D^0 tracks (t) are constrained to come from a common vertex and the D^0 and slow pion are constrained to form a common vertex within the beam interaction region. The χ^2 probabilities of the D^0 and D^* vertices from this fit must be at least 1%. The reconstructed D^0 mass $m(D^0)$ must be within [1.65, 2.05] GeV and the mass difference Δm must be within [0.141, 0.149] GeV. We subtract a data–Monte Carlo difference of 0.91 ± 0.06 MeV, measured in the $D^0 \to \pi^+\pi^-$ sample, from the reconstructed D^0 mass in the simulation.

We use an error-correcting output code (ECOC) algorithm [7] with 36 input variables to identify electrons and pions. The ECOC combines multiple bootstrap aggregated [8] decision tree [9] binary classifiers trained to separate e, π, K, and p. The most important inputs for electron identification are the EMC energy divided by the track momentum, several EMC shower shape variables, and the deviation from the expected value divided by the measurement uncertainty for the Cherenkov angle and dE/dx for the e, π, K, and p hypotheses. For tracks with momentum greater than 0.5 GeV, the electron identification has an efficiency of 95% for electrons and a pion misidentification probability of less than 0.2%. Neutral clusters in the EMC that are consistent with bremsstrahlung radiation are used to correct the momentum and energy of electron candidates. The efficiency of the pion identification is above 90% for pions, with a kaon misidentification probability below 10%.

Muons are identified using a bootstrap aggregated decision tree algorithm with 30 input variables. Of these, the most important are the number and positions of the hits in the IFR, the difference between the measured and expected DCH dE/dx for the muon hypothesis, and the energy deposited in the EMC. For tracks with momentum greater than 1 GeV, the muon identification has an efficiency of about 60% for muons, with a pion misidentification probability of between 0.5% and 1.5%.

The reconstruction efficiencies for the different channels after the above particle identification requirements are about 18% for e^+e^-, 9% for $\mu^+\mu^-$, 13% for $e^\pm\mu^\mp$, and 26% for $\pi^+\pi^-$. The background candidates that remain are either random combinations of two leptons (combinatorial background) or $D^0 \to \pi^+\pi^-$ decays where both pions pass the lepton identification criteria (peaking background). The $D^0 \to \pi^+\pi^-$ background is most important for the $D^0 \to \mu^+\mu^-$ channel.

Figure 1 shows the reconstructed invariant mass distributions from Monte Carlo (MC) simulated samples for the three $D^0 \to \ell^+\ell^-$ signal channels. Also shown are the distributions from $D^0 \to \pi^+\pi^-$ reconstructed as $D^0 \to \ell^+\ell^-$ and $D^0 \to K^-\pi^+$ reconstructed as $D^0 \to \ell^+\ell^-$ for each signal channel. The overlap between the $D^0 \to \ell^+\ell^-$ and $D^0 \to \pi^+\pi^-$ distributions is largest for the $D^0 \to \mu^+\mu^-$ channel, while the $D^0 \to \ell^+\ell^-$ and $D^0 \to K^-\pi^+$ distributions are well separated.

The combinatorial background originates mostly from events with two semileptonic B and/or D decays. The sample of events selected by the above criteria are dominantly from $e^+e^- \to B\bar{B}$ events, rather than events from the $e^+e^- \to q\bar{q}$ ($q = u, d, s, c$) continuum. We use a linear combination (Fisher discriminant [10]) of the following five variables to reduce the combinatorial $B\bar{B}$ background:

(i) The measured D^0 flight length divided by its uncertainty.

(ii) The value of $|\cos\theta_{\rm hel}|$, where $\theta_{\rm hel}$ is defined as the angle between the momentum of the positively charged D^0 daughter and the boost direction from the lab frame to the D^0 rest frame, all in the D^0 rest frame.

(iii) The missing transverse momentum with respect to the beam axis.

(iv) The ratio of the second and zeroth Fox–Wolfram moments [11].

(v) The D^0 momentum in the CM frame.

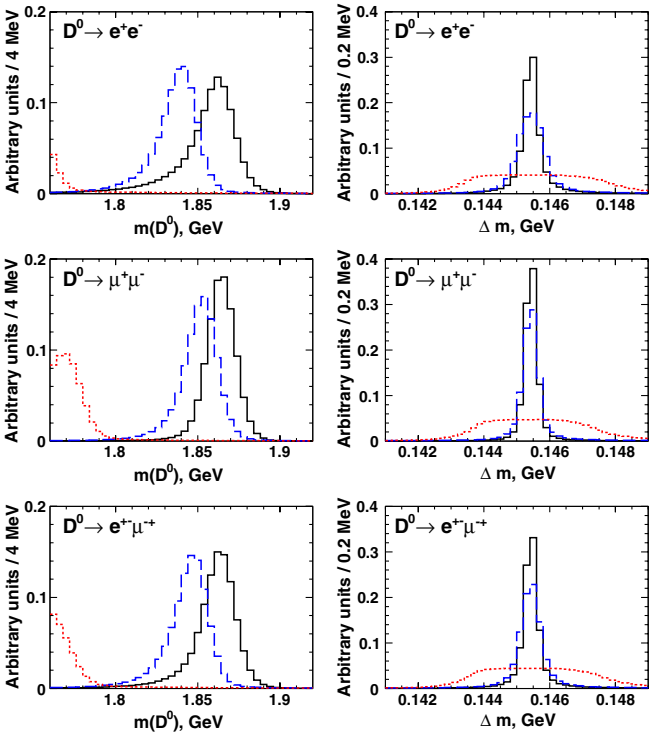

FIG. 1 (color online). Reconstructed D^0 mass (left) and Δm (right) for the three signal channels: $D^0 \to e^+e^-$ (top), $D^0 \to \mu^+\mu^-$ (middle), and $D^0 \to e^\pm\mu^\mp$ (bottom). The solid (black) histogram is the signal MC sample, the dashed (blue) histogram is the $D^0 \to \pi^+\pi^-$ MC sample reconstructed as $D^0 \to \ell^+\ell^-$, and the dotted (red) histogram is the $D^0 \to K^-\pi^+$ MC sample reconstructed as $D^0 \to \ell^+\ell^-$. The $D^0 \to \ell^+\ell^-$ and $D^0 \to \pi^+\pi^-$ distributions have been normalized to unit area. The $D^0 \to K^-\pi^+$ normalization is arbitrary.

The flight length for the combinatorial background is symmetric about zero, while the signal has an exponential distribution. The $|\cos\theta_{\rm hel}|$ distribution is uniform for the signal but peaks at zero for the combinatorial $B\bar{B}$ background. The neutrinos from the semileptonic decays in $B\bar{B}$ background events create missing transverse momentum, while there is none for signal events. The ratio of Fox–Wolfram moments uses general event-shape information to separate $B\bar{B}$ and continuum $q\bar{q}$ events. Finally, the signal has a broad D^0 CM momentum spectrum that peaks at about 3 GeV, while the combinatorial background peaks at the minimum allowed value of 2.4 GeV.

Figure 2 shows distributions of the Fisher discriminant ($\mathcal{F}$) for samples of $B\bar{B}$ MC, $D^0 \to \mu^+\mu^-$ signal MC, and continuum background MC. The separation between signal and $B\bar{B}$ background distributions is large, while the signal and continuum background distributions are similar. For example, requiring $\mathcal{F}$ to be greater than 0 removes about 90% of the $B\bar{B}$ background while keeping 85% of the signal. The minimum $\mathcal{F}$ value is optimized for each signal channel as described below.

We use the $|\cos\theta_{\rm hel}|$ variable directly to remove the continuum combinatorial background. Figure 3 shows distributions of $|\cos\theta_{\rm hel}|$ before making a minimum $\mathcal{F}$ requirement, for $B\bar{B}$ background, continuum background, and signal. The dropoff for $|\cos\theta_{\rm hel}|$ near 1.0 in the signal distributions is caused by the selection and particle identification requirements. The $B\bar{B}$ background peaks near zero, while the continuum background peaks sharply near one.

The selection criteria for each signal channel were chosen to give the lowest expected signal branching

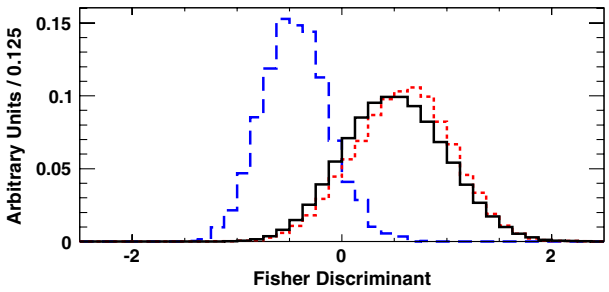

FIG. 2 (color online). Fisher discriminant, $\mathcal{F}$, distributions for the $B\bar{B}$ MC sample (dashed blue line), the $D^0 \to \mu^+\mu^-$ signal MC sample (solid black line), and the continuum MC sample (dotted red line). The $\mathcal{F}$ distributions for $D^0 \to e^+e^-$ and $D^0 \to e^\pm\mu^\mp$ are similar to those of $D^0 \to \mu^+\mu^-$.

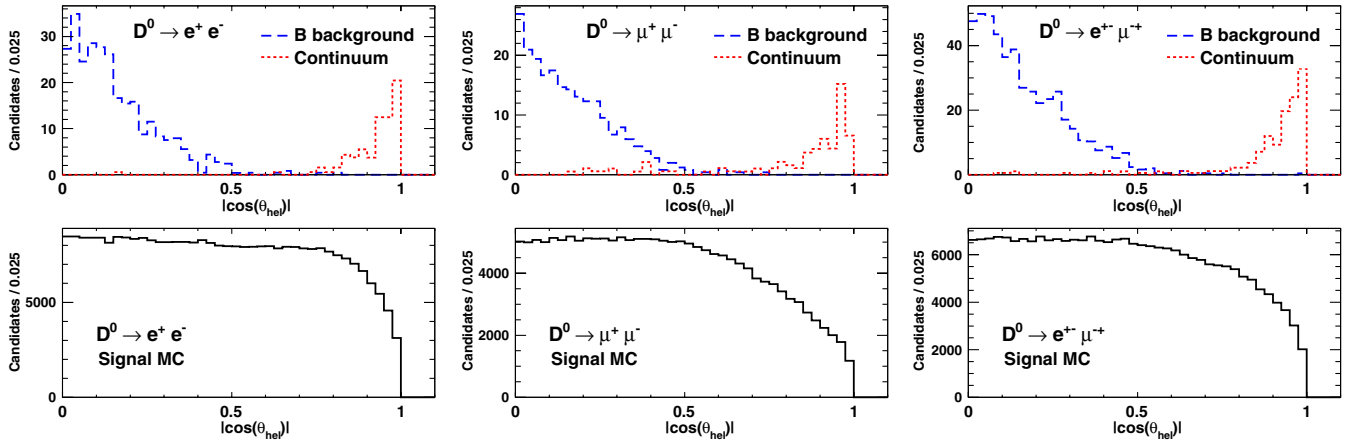

FIG. 3 (color online). Distributions of $|\cos(\theta_{\rm hel})|$ for the three signal channels: $D^0 \to e^+e^-$ (left), $D^0 \to \mu^+\mu^-$ (center), and $D^0 \to e^\pm\mu^\mp$ (right). The top distributions show Monte Carlo distributions for the combinatorial $B\bar{B}$ (dashed blue lines) and continuum (dotted red lines) backgrounds. The bottom distributions show the signal Monte Carlo samples with arbitrary normalization.

fraction upper limit for the null hypothesis (a true branching fraction of zero) using the MC samples. The Fisher discriminant coefficients were determined before applying the $|\cos\theta_{\rm hel}|$, D^0 mass, and Δm requirements. We then tested a total of 2700 configurations of $|\cos\theta_{\rm hel}|$, $\mathcal{F}$, D^0 mass, and Δm criteria. Table I summarizes the resulting best values for the maximum $|\cos\theta_{\rm hel}|$, minimum $\mathcal{F}$, $m(D^0)$ signal window, and Δm interval.

After the selection criteria in Table I were determined, the data yields in the sideband region were compared to the expectations from Monte Carlo samples. The $D^0 \to \mu^+\mu^-$ and $D^0 \to e^\pm\mu^\mp$ data yields were consistent with the expectations from the Monte Carlo samples. However, the $D^0 \to e^+e^-$ sideband yield showed a substantial excess of events; 90 events were observed when 5.5 ± 1.6 were expected.

The excess of data sideband events over the expected background from Monte Carlo samples was investigated and found to have several distinct features: low track multiplicity, event-shape characteristics that are similar to continuum events, tracks consistent with electrons produced in photon conversions, low D^0 daughter track momenta, and undetected energy along the beam axis. We found that such events result from hard initial state radiation events or two-photon interaction processes that are not simulated in the continuum MC samples used in the analysis. The following selection criteria were added in order to remove such background contributions:

(i) Events must have at least five tracks for the $D^0 \to e^+e^-$ channel and at least four tracks for the $D^0 \to \mu^+\mu^-$ and $D^0 \to e^\pm\mu^\mp$ channels.
(ii) Events can have at most three electron candidates.
(iii) The longitudinal boost of the event, reconstructed from all tracks and neutral clusters, along the high-energy beam direction p_z/E in the CM frame must be greater than -0.5 for all three $D^0 \to \ell^+\ell^-$ channels.
(iv) For $D^0 \to \mu^+\mu^-$ and $D^0 \to e^\pm\mu^\mp$ candidates, the pion track from the D^{*+} decay and the leptons must be inconsistent with originating from a photon conversion.

TABLE I. Selection criteria for the three $D^0 \to \ell^+\ell^-$ signal decay modes. The parameter in the last row is defined as $\delta\Delta m \equiv \Delta m - \Delta m_0$, where Δm_0 is the nominal $D^{*+} - D^0$ mass difference [12].

Parameter	e^+e^-	$\mu^+\mu^-$	$e^\pm\mu^\mp$
$\lvert\cos\theta_{\rm hel}\rvert$	<0.85	<0.90	<0.85
$\mathcal{F}$	>0.00	>-0.25	>0.00
$m(D^0)$ (GeV)	[1.815, 1.890]	[1.855, 1.890]	[1.845, 1.890]
$\lvert\delta\Delta m\rvert$ (MeV)	<0.5	<0.5	<0.4

The signal efficiencies for the $D^0 \to e^+e^-$, $D^0 \to \mu^+\mu^-$, and $D^0 \to e^\pm\mu^\mp$ channels for these additional criteria are 91.4%, 99.3%, and 96.8%, respectively. The $D^0 \to e^+e^-$ sideband yield in the data with these criteria applied is reduced to eight events where 4.5 ± 1.3 are expected, based on the Monte Carlo samples.

A. Peaking $D^0 \to \pi^+\pi^-$ background estimation

The amount of $D^0 \to \pi^+\pi^-$ peaking background within the $m(D^0)$ signal window is estimated from data and calculated separately for each $D^0 \to \ell^+\ell^-$ channel using

$$N^{\rm BG}_{\pi\pi} = \left(\sum_i N^{NP}_{\pi\pi,i} \cdot \langle p^+_{f,i}\rangle\langle p^-_{f,i}\rangle\right) \cdot \epsilon_{m(D^0)} \cdot G, \qquad (1)$$

where the sum i is over the six data-taking periods, $N^{NP}_{\pi\pi,i}$ is the number of $D^0 \to \pi^+\pi^-$ events that pass all of the $D^0 \to \ell^+\ell^-$ selection criteria except for the lepton identification and $m(D^0)$ signal window requirements, $\langle p^+_{f,i}\rangle \times \langle p^-_{f,i}\rangle$ is the product of the average probability that the π^+

and the π^- pass the lepton identification criteria, $\epsilon_{m(D^0)}$ is the efficiency for $D^0 \to \pi^+\pi^-$ background to satisfy the $m(D^0)$ signal window requirement, and G takes into account a positive correlation in the probability that the π^+ and the π^- pass the muon identification criteria. The value of $\langle p^+_{f,i}\rangle$ ($\langle p^-_{f,i}\rangle$) is measured using the ratio of the $D^0 \to \pi^+\pi^-$ yield requiring that the π^+ (π^-) satisfy the lepton identification requirements to the $D^0 \to \pi^+\pi^-$ yield with no lepton identification requirements applied. The $\langle p^+_{f,i}\rangle$ and $\langle p^-_{f,i}\rangle$ are measured separately for each of the six major data-taking periods due to the changing IFR performance with time. The values of $\langle p^+_{f,i}\rangle$ and $\langle p^-_{f,i}\rangle$ vary between 0.5% and 1.5%. The probability that the π^+ and π^- both pass the muon identification criteria is enhanced when the two tracks curve toward each other, instead of away from each other, in the plane perpendicular to the beam axis. We use $G = 1.19 \pm 0.05$ for the $D^0 \to \mu^+\mu^-$ channel and $G = 1$ for the $D^0 \to e^+e^-$ and $D^0 \to e^\pm\mu^\mp$ channels. The G factor is measured using a high-statistics $D^0 \to K^-\pi^+$ sample where the K is required to have a signature in the IFR that matches that of a π, which passes the μ identification criteria. This is in good agreement with the MC estimate of the G factor value, 1.20 ± 0.10.

B. Combinatorial background estimation

The combinatorial background is estimated by using the number of observed events in a sideband region and the expected ratio of events $R_{\rm cb}$ in the signal and sideband regions, determined from MC simulation. The sideband is above the signal region in the D^0 mass ([1.90, 2.05] GeV) in a wide Δm window ([0.141, 0.149] GeV). We fit the D^0 mass and Δm projections of the combinatorial background MC using second-order polynomials. A two-dimensional probability density function (PDF) is formed by multiplying the one-dimensional PDFs, assuming the variables are uncorrelated. The combinatorial background signal-to-sideband ratio $R_{\rm cb}$ is then computed from the ratio of the integrals of the two-dimensional PDF.

III. RESULTS

The distribution of Δm vs D^0 mass as well as projections of Δm and the D^0 mass for the data events for the three signal channels are shown in Fig. 4. Peaks from $D^0 \to K^-\pi^+$ and $D^0 \to \pi^+\pi^-$ are visible at 1.77 GeV and 1.85 GeV in the D^0 mass distribution for $D^0 \to \mu^+\mu^-$ candidates. We observe 1, 8, and 2 events in the $D^0 \to e^+e^-$, $D^0 \to \mu^+\mu^-$, and $D^0 \to e^\pm\mu^\mp$ signal regions, respectively.

A. $D^0 \to \ell^+\ell^-$ branching fractions

The yield of $D^0 \to \pi^+\pi^-$ decays in the $\pi\pi$ control sample, selected with the same $\mathcal{F}$ and $|\cos\theta_{\rm hel}|$ criteria for each $D^0 \to \ell^+\ell^-$ signal mode (see Table I), is used to normalize the $D^0 \to \ell^+\ell^-$ signal branching fraction. For each $D^0 \to \ell^+\ell^-$ signal channel, the $D^0 \to \pi^+\pi^-$ yield $N^{\rm fit}_{\pi\pi}$ is determined by fitting the D^0 mass spectrum of the $D^0 \to \pi^+\pi^-$ control sample in the range [1.7, 2.0] GeV. The fit has three components: $D^0 \to \pi^+\pi^-$, $D^0 \to K^-\pi^+$, and combinatorial background. The PDF for the $D^0 \to \pi^+\pi^-$ component is the sum of a Crystal Ball function and two Gaussians. The Crystal Ball function is a Gaussian modified to have an extended, power-law tail on the low side [13]. The PDF for the $D^0 \to K^-\pi^+$ component is the sum of a Crystal Ball function and an exponential function. The combinatorial background PDF is an exponential function.

The $D^0 \to \ell^+\ell^-$ branching fraction is given by

$$\mathcal{B}_{\ell\ell} = \left(\frac{N_{\ell\ell}}{N^{\rm fit}_{\pi\pi}}\right)\left(\frac{\epsilon_{\pi\pi}}{\epsilon_{\ell\ell}}\right)\mathcal{B}_{\pi\pi} = S_{\ell\ell}\cdot N_{\ell\ell}, \qquad (2)$$

where $N_{\ell\ell}$ is the number of $D^0 \to \ell^+\ell^-$ signal candidates, $N^{\rm fit}_{\pi\pi}$ is the number of $D^0 \to \pi^+\pi^-$ candidates from the fit, $\epsilon_{\pi\pi}$ and $\epsilon_{\ell\ell}$ are the efficiencies for the corresponding decay modes, $\mathcal{B}_{\pi\pi} = (1.400 \pm 0.026)\times 10^{-3}$ is the $D^0 \to \pi^+\pi^-$ branching fraction [12], and $S_{\ell\ell}$ is defined by

$$S_{\ell\ell} \equiv \frac{\mathcal{B}_{\pi\pi}}{N^{\rm fit}_{\pi\pi}}\frac{\epsilon_{\pi\pi}}{\epsilon_{\ell\ell}}. \qquad (3)$$

The expected observed number of events in the signal region is given by

$$N_{\rm obs} = \mathcal{B}_{\ell\ell}/S_{\ell\ell} + N_{\rm BG}. \qquad (4)$$

The uncertainties on $S_{\ell\ell}$ and $N_{\rm BG}$ are incorporated into a likelihood function by convolving a Poisson PDF in $N_{\rm obs}$ with Gaussian PDFs in $S_{\ell\ell}$ and $N_{\rm BG}$. We determine 90% confidence level intervals using the likelihood ratio ordering principle of Feldman and Cousins [14] to construct the confidence belts. The estimated branching fractions and 1 standard deviation uncertainties are determined from the values of $\mathcal{B}_{\ell\ell}$ that maximize the likelihood and give a change of 0.5 in the log likelihood relative to the maximum, respectively.

B. Systematic uncertainties

Table II summarizes the systematic uncertainties. Several of the uncertainties in $\epsilon_{\pi\pi}/\epsilon_{\ell\ell}$ cancel, including tracking efficiency for the D^0 daughters, slow pion efficiency, and the efficiencies of the $\mathcal{F}$ and D^0 momentum requirements. The uncertainty on $\epsilon_{\pi\pi}/\epsilon_{\ell\ell}$ due to particle identification is 4%. Bremsstrahlung creates a low-side tail in the D^0 mass distributions for the $D^0 \to e^+e^-$ and $D^0 \to e^\pm\mu^\mp$ decay modes. The uncertainty $\epsilon_{\ell\ell}$ due to the modeling of this tail is 3% for $D^0 \to e^+e^-$ and 2% for $D^0 \to e^\pm\mu^\mp$. The Crystal Ball shape parameters that describe the low-side tail of the D^0 mass distribution were varied, leading to an uncertainty of 1.1% to 1.3% on $N^{\rm fit}_{\pi\pi}$. We use the world average for the $D^0 \to \pi^+\pi^-$ branching fraction [12], which has an uncertainty of 1.9%. We

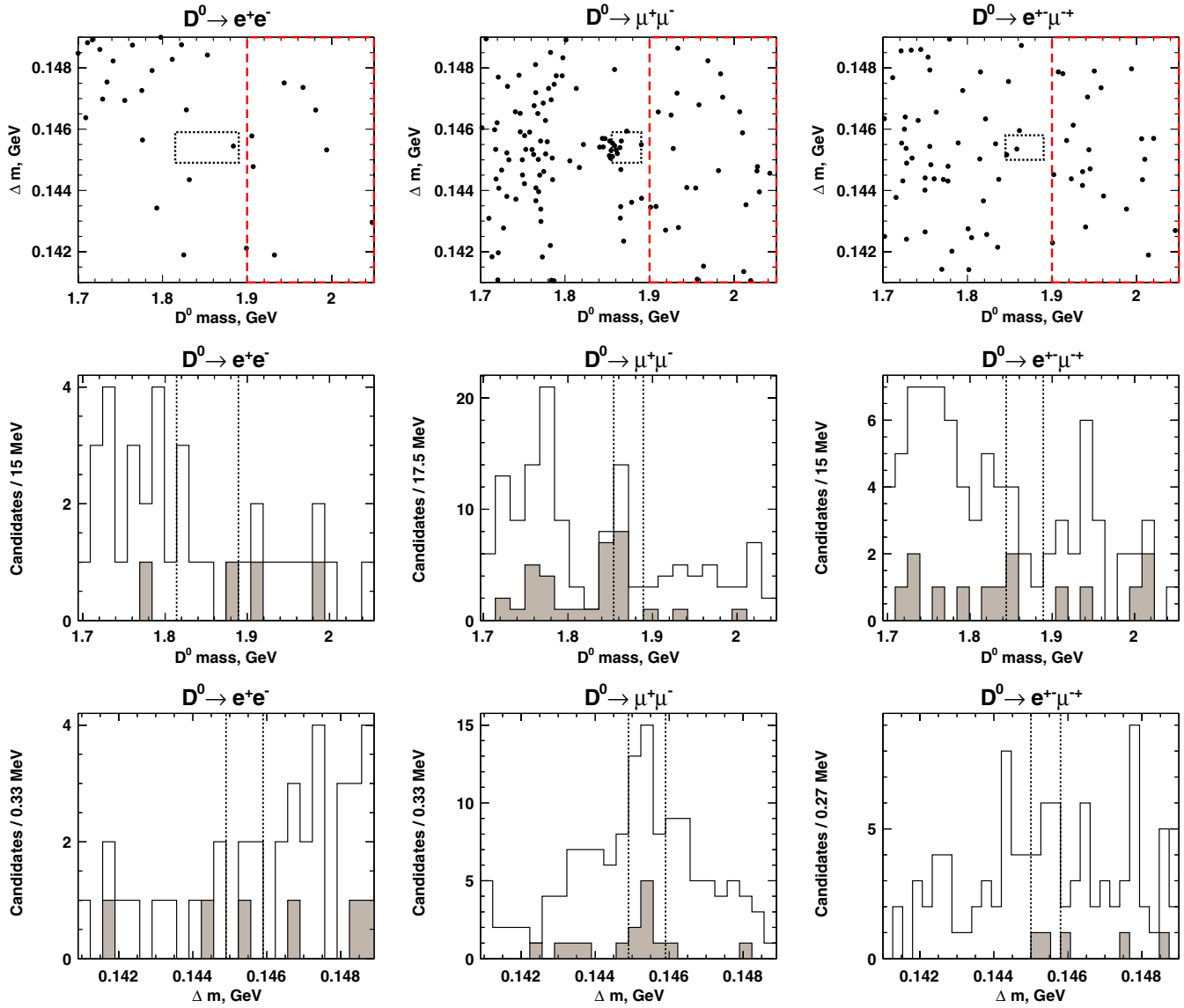

FIG. 4 (color online). Data distributions of Δm vs the reconstructed D^0 mass (top row), projections of the D^0 mass (middle row), and Δm (bottom row). The columns contain the distributions for the $D^0 \to e^+e^-$ (left), $D^0 \to \mu^+\mu^-$ (center), and $D^0 \to e^\pm\mu^\mp$ (right) decay modes. The shaded D^0 mass (Δm) distributions represent the subset of events that fall in the Δm (D^0 mass) signal window. In the top row, the dotted (black) box indicates the signal region and the dashed (red) box indicates the sideband region. In the middle and bottom rows, the vertical dotted black lines indicate the boundaries of the signal region.

TABLE II. Systematic uncertainties. The uncertainty on $S_{\ell\ell}$ results from the uncertainties on $\epsilon_{\pi\pi}/\epsilon_{\ell\ell}$, $N_{\pi\pi}^{\rm fit}$, and $\mathcal{B}_{\pi\pi}$ added in quadrature. The systematic uncertainty on the overall background $N_{\rm BG}$ is obtained from the uncertainties on $N_{\pi\pi}^{\rm BG}$ and $N_{\rm cb}$ added in quadrature.

	$D^0 \to e^+e^-$	$D^0 \to \mu^+\mu^-$	$D^0 \to e^\pm\mu^\mp$
$\epsilon_{\pi\pi}/\epsilon_{\ell\ell}$, particle ID	4%	4%	4%
$\epsilon_{\pi\pi}/\epsilon_{\ell\ell}$, bremsstrahlung	3%	-	2%
$N_{\pi\pi}^{\rm fit}$	1.2%	1.3%	1.1%
$\mathcal{B}_{\pi\pi}$	1.9%	1.9%	1.9%
$S_{\ell\ell}$	5.4%	4.6%	5.0%
$N_{\pi\pi}^{\rm BG}$	11% (0.004 events)	16% (0.43 events)	5%
$N_{\rm cb}$, $R_{\rm cb}$	36% (0.35 events)	20% (0.25 events)	19% (0.20 events)
$N_{\rm BG}$	0.35 events	0.50 events	0.20 events

combine the above relative uncertainties in quadrature resulting in 4.6% to 5.4% systematic uncertainties on $S_{\ell\ell}$.

The D^0 mass range for the fit used to determine the combinatorial background PDF was varied from [1.70, 2.05] GeV to [1.80, 2.05] GeV. The difference in the resulting signal-to-sideband ratio $R_{\rm cb}$ is taken as a systematic uncertainty. The pion misidentification probabilities for e and μ measured in data are in good agreement with the MC simulation. We use the larger of either the difference between the data and the MC or the statistical uncertainty on the MC misidentification probabilities as a systematic uncertainty. For the $D^0 \to \mu^+\mu^-$ decay mode, we take the uncertainty on the MC estimate for the G factor of 8% as a systematic uncertainty on the G estimate from the $D^0 \to K^-\pi^+$ data control sample.

C. Branching fraction results

Table III presents the results, where $N_{\rm SB}$ is the number of events in the upper sideband, $N_{\rm cb}$ is the expected number of combinatorial background events in the signal window, $N_{\pi\pi}^{\rm BG}$ is the number of events from the $D^0 \to \pi^+\pi^-$ peaking background, and $N_{\rm BG}$ (data) is the expected number of total background events in the data.

For the $D^0 \to e^+e^-$ and $D^0 \to e^\pm\mu^\mp$ channels, the event yield in the signal region is consistent with background only. We observe one and two events with expected backgrounds of 1.0 ± 0.5 and 1.4 ± 0.3 events for the $D^0 \to e^+e^-$ and $D^0 \to e^\pm\mu^\mp$ channels, respectively. The 90% confidence interval upper limits for the branching fractions are $<1.7 \times 10^{-7}$ for $D^0 \to e^+e^-$ and $<3.3 \times 10^{-7}$ for $D^0 \to e^\pm\mu^\mp$.

For the $D^0 \to \mu^+\mu^-$ channel, we observe 8 events in the signal region, where we expect 3.9 ± 0.6 background events. There is a cluster of $D^0 \to \mu^+\mu^-$ candidate events in Fig. 4 just above and below the lower D^0 mass edge of the signal region, where the $D^0 \to \pi^+\pi^-$ background is expected. We expect 7.5 ± 0.8 $D^0 \to \pi^+\pi^-$ events in the entire [1.7, 2.05] GeV D^0 mass range, with 93% of these events falling within the narrower [1.830, 1.875] GeV range. The combinatorial background in the [1.830, 1.875] GeV D^0 mass interval is expected to be 1.8 ± 0.6 events, giving a total expected background of 8.8 ± 1.1 events. In this interval, we observe 15 events. The probability of observing 15 or more events when 8.8 ± 1.1 events are expected is 4.6%, which corresponds to a 1.7 standard deviation upward fluctuation from the mean for a Gaussian distribution [i.e. $(\mathrm{Erf}(1.7/\sqrt{2})+1)/2 = 1 - 0.046$]. The probability of observing 8 events when 3.9 ± 0.6 events are expected is 5.4%. We conclude that the excess over the expected background is not statistically significant. The Feldman–Cousins method results in a two-sided 90% confidence interval for the $D^0 \to \mu^+\mu^-$ branching fraction of $[0.6, 8.1] \times 10^{-7}$.

In summary, we have searched for the leptonic charm decays $D^0 \to e^+e^-$, $D^0 \to \mu^+\mu^-$, and $D^0 \to e^\pm\mu^\mp$ using 468 fb^{-1} of integrated luminosity recorded by the *BABAR* experiment. We find no statistically significant excess over the expected background. These results supersede our previous results [15] and are consistent with the results of the Belle experiment [16], which has set 90% confidence level upper limits of $<0.79 \times 10^{-7}$, $<1.4 \times 10^{-7}$, and $<2.6 \times 10^{-7}$, for the $D^0 \to e^+e^-$, $D^0 \to \mu^+\mu^-$, and

TABLE III. Results for the observed event yields ($N_{\rm obs}$), estimated background ($N_{\rm BG}$), and signal branching fractions ($\mathcal{B}_{\ell\ell}$). The branching fraction 90% confidence interval (C.I.) is given in the last row of the table. The first uncertainty is statistical and the second systematic. $N_{\rm SB}$ is the observed number of events in the sideband, $R_{\rm cb}$ is the signal-to-sideband ratio for combinatorial background, $N_{\rm cb}$ and $N_{\pi\pi}^{\rm BG}$ are the estimated combinatorial and $D^0 \to \pi^+\pi^-$ backgrounds in the signal region, $N_{\pi\pi}^{\rm fit}$ is the fitted yield in the $D^0 \to \pi^+\pi^-$ control sample, $\epsilon_{\pi\pi}$ and $\epsilon_{\ell\ell}$ are the $\pi\pi$ control sample and signal selection efficiencies, determined from Monte Carlo samples, which have negligible statistical uncertainties. The systematic uncertainty on $\epsilon_{\pi\pi}/\epsilon_{\ell\ell}$ is included in the systematic uncertainty on $S_{\ell\ell}$, which is defined in Eq. (3).

	$D^0 \to e^+e^-$	$D^0 \to \mu^+\mu^-$	$D^0 \to e^\pm\mu^\mp$
$N_{\rm SB}$	8	27	24
$R_{\rm cb}$	$0.121 \pm 0.023 \pm 0.044$	$0.046 \pm 0.005 \pm 0.009$	$0.042 \pm 0.006 \pm 0.008$
$N_{\rm cb}$	$0.97 \pm 0.39 \pm 0.35$	$1.24 \pm 0.27 \pm 0.25$	$1.00 \pm 0.25 \pm 0.20$
$N_{\pi\pi}^{\rm BG}$	$0.037 \pm 0.012 \pm 0.004$	$2.64 \pm 0.22 \pm 0.43$	$0.42 \pm 0.08 \pm 0.02$
$N_{\rm BG}$	$1.01 \pm 0.39 \pm 0.35$	$3.88 \pm 0.35 \pm 0.50$	$1.42 \pm 0.26 \pm 0.20$
$N_{\pi\pi}^{\rm fit}$	$39930 \pm 210 \pm 490$	$51800 \pm 240 \pm 660$	$39840 \pm 210 \pm 430$
$\epsilon_{\pi\pi}$	14.4%	18.7%	14.6%
$\epsilon_{\ell\ell}$	9.48%	6.29%	6.97%
$S_{\ell\ell}(\times 10^{-9})$	$53.4 \pm 0.2 \pm 2.9$	$80.6 \pm 0.4 \pm 3.7$	$73.9 \pm 0.4 \pm 3.7$
$N_{\rm obs}$	1	8	2
$\mathcal{B}_{\ell\ell}(\times 10^{-7})$	$0.1^{+0.7}_{-0.4}$	$3.3^{+2.6}_{-2.0}$	$0.5^{+1.3}_{-0.9}$
$\mathcal{B}_{\ell\ell}(\times 10^{-7})$ 90% C.I.	<1.7	[0.6, 8.1]	<3.3

$D^0 \to e^{\pm}\mu^{\mp}$ branching fractions, respectively. The LHCb experiment has recently presented preliminary search results [17] for $D^0 \to \mu^+\mu^-$, where they find no evidence for this decay and set an upper limit on the branching fraction of $<1.3 \times 10^{-8}$ at 95% confidence level.

ACKNOWLEDGMENTS

We are grateful for the extraordinary contributions of our PEP-II colleagues in achieving the excellent luminosity and machine conditions that have made this work possible. The success of this project also relies critically on the expertise and dedication of the computing organizations that support *BABAR*. The collaborating institutions wish to thank SLAC for its support and the kind hospitality extended to them. This work is supported by the U.S. Department of Energy and National Science Foundation, the Natural Sciences and Engineering Research Council (Canada), the Commissariat à l'Energie Atomique and Institut National de Physique Nucléaire et de Physique des Particules (France), the Bundesministerium für Bildung und Forschung and Deutsche Forschungsgemeinschaft (Germany), the Istituto Nazionale di Fisica Nucleare (Italy), the Foundation for Fundamental Research on Matter (Netherlands), the Research Council of Norway, the Ministry of Education and Science of the Russian Federation, Ministerio de Ciencia e Innovación (Spain), and the Science and Technology Facilities Council (United Kingdom). Individuals have received support from the Marie-Curie IEF program (European Union) and the A. P. Sloan Foundation (USA).

[1] G. Burdman, E. Golowich, J. A. Hewett, and S. Pakvasa, Phys. Rev. D **66**, 014009 (2002).
[2] E. Golowich, J. A. Hewett, S. Pakvasa, and A. A. Petrov, Phys. Rev. D **79**, 114030 (2009).
[3] PEP-II Conceptual Design Report. No. SLAC-0418, 1993.
[4] B. Aubert *et al.* (*BABAR* Collaboration), Nucl. Instrum. Methods Phys. Res., Sect. A **479**, 1 (2002).
[5] W. Menges, IEEE Nucl. Sci. Symp. Conf. Rec. **3**, 1470 (2006).
[6] The use of charge conjugate processes is implied unless explicitly stated otherwise.
[7] T. G. Dietterich and G. Bakiri, J. Artif. Intell. Res. **2**, 263 (1995).
[8] L. Breiman, Mach. Learn. **24**, 123 (1996).
[9] L. Breiman, J. Friedman, C. Stone, and R. A. Olshen, *Classification and Regression Trees* (CRC Press, Boca Raton, FL, 1984).
[10] R. A. Fisher, Ann. Eugenics **7**, 179 (1936).
[11] G. C. Fox and S. Wolfram, Phys. Rev. Lett. **41**, 1581 (1978).
[12] K. Nakamura *et al.* (Particle Data Group), J. Phys. G **37**, 075021 (2010).
[13] M. J. Oreglia, Ph.D. thesis, Stanford University [Report No. SLAC-R-236, 1980]; J. E. Gaiser, Ph.D. thesis, Stanford University [Report No. SLAC-R-255, 1982].
[14] G. J. Feldman and R. D. Cousins, Phys. Rev. D **57**, 3873 (1998).
[15] B. Aubert *et al.* (*BABAR* Collaboration), Phys. Rev. Lett. **93**, 191801 (2004).
[16] M. Petric *et al.* (Belle Collaboration), Phys. Rev. D **81**, 091102(R) (2010).
[17] W. Bonivento *et al.* (LHCb Collaboration), in Proceedings 6 of the 47th Rencrontres de Moriond on Electroweak Interactions and Unified Theories, La Thuile, Italy, 2012 [Report No. LHCb-CONF-2012-005].